

# The electrochemical corrosion behaviour of quaternary gold alloys when exposed to 3.5 % NaCl solution

L. P. Ward · D. Chen · A. P. O'Mullane

Published online: 10 January 2013

© The Author(s) 2013. This article is published with open access at SpringerLink.com

**Abstract** Lower carat gold alloys, specifically 9 carat gold alloys, containing less than 40 % gold, and alloying additions of silver, copper and zinc, are commonly used in many jewellery applications, to offset high costs and poor mechanical properties associated with pure gold. While gold is considered to be chemically inert, the presence of active alloying additions raises concerns about certain forms of corrosion, particularly selective dissolution of these alloys. The purpose of this study was to systematically study the corrosion behaviour of a series of quaternary gold–silver–copper–zinc alloys using dc potentiodynamic scanning in saline (3.5 % NaCl) environment. Full anodic/cathodic scans were conducted to determine the overall corrosion characteristics of the alloy, followed by selective anodic scans and subsequent morphological and compositional analysis of the alloy surface and corroding media to determine the extent of selective dissolution. Varying degrees of selective dissolution and associated corrosion rates were observed after anodic polarisation in 3.5 % NaCl, depending on the alloy composition. The corrosion behaviour of the alloys was determined by the extent of anodic reactions which induce (1) formation of oxide scales on the alloy surface and or (2) dissolution of Zn and Cu species. In general, the improved corrosion characteristics of alloy #3 was attributed to the composition of Zn/Cu in the alloy and thus favourable microstructure promoting the formation of

protective oxide/chloride scales and reducing the extent of Cu and Zn dissolution.

**Keywords** Gold alloy · 3.5 % NaCl · Potentiodynamic scanning · Anodic polarisation · Characterisation · Selective dissolution

## Introduction

The inherent physical properties of gold, including electrical conductivity and chemical inertness combined with attractive appearance, have established its use in a number of areas, such as the electronics, dental and jewellery industries. However, pure (24 carat) gold is expensive and mechanically weak (soft) and therefore has limited applications even in jewellery applications. Consequently, attention has focussed on the development of a range of lower carat gold alloys, particularly 9 carat gold alloys, where compositions vary from ternary gold–silver–copper alloys to quaternary alloys where zinc is added primarily to improve workability through contraction of the two-phase field of the phase diagram [1] and to a lesser extent counteract the red colour induced by copper [2].

In order to function satisfactorily in jewellery applications, certain requirements have to be met with respect to mechanical, chemical and biological properties, particularly where prolonged contact with human skin is evident. Gold itself is considered chemically inert and biologically compatible with the body. However, there is concern with respect to the corrosive nature of these gold alloys, particularly the lower carat, quaternary alloys where the presence of non-noble metals in the alloy are likely to strongly influence the corrosion resistance.

Rapson [3] has reported that the significant areas where corrosion and tarnishing of gold alloys becomes important are (1) tarnishing of gold electrical contacts and gold jewellery; (2) corrosion of gold dental alloys and gold jewellery

L. P. Ward (✉)

School of Civil, Environmental and Chemical Engineering,  
RMIT University, Melbourne, VIC, Australia  
e-mail: liam.ward@rmit.edu.au

D. Chen

Department of Chemistry and Chemical Engineering,  
Foshan University, Foshan, Guangdong, China

A. P. O'Mullane

School of Applied Sciences, RMIT University,  
Melbourne, VIC, Australia

and (3) stress corrosion cracking of gold jewellery. Gold jewellery is known to corrode in a number of environments which include sea water and chlorinated water.

Numerous studies have been conducted on the mechanisms and consequential effects of stress corrosion cracking (SCC), a well-known form of environmental attack in low carat gold jewellery, particularly below 14 carat gold content [3–10]. While there appears to be less information available on other forms of corrosion, such as pitting and intergranular corrosion, the concepts of selective leaching of alloying elements to modify alloys for decorative purposes has been around for many years [11, 12]. Her, gold alloys are depleted intentionally of alloying elements to produce “gold of higher purity”. Copper depletion with the aid of acid plant juices was practiced by the ancient South Americans [11] and Forty [12] referred to the production of a gold-rich surface from a gold–silver alloy as far back as the twelfth century through the selective corrosion of the less noble species using nitric acid. The electrochemical corrosion behaviour of a series of Au–Cu–Ag–Pd alloys and the metallurgical dependence has been studied by Nakagawa [13] who reported that single-phase alloys showed superior corrosion resistance than the dual-phase alloys. Forty [14] has studied the selective dissolution of active constituents in gold alloys and found that selective dissolution is more likely to occur in the lower carat gold alloys. Laub and Stanford [15] reported that for ternary Au–Ag–Cu alloys, both copper and silver were involved in the corrosion process; corrosion occurring primarily in the silver-rich regions and secondarily in the copper-rich regions. Fujita and co-workers [16] observed for an Ag–Au–Pt–Cu alloy, comprising of a mixture of a major phase of the matrix and minor phase of small grains embedded in the matrix, corrosion occurred preferentially in the matrix and not the precipitates. It was suggested that  $\text{Ag}^+$  ions were released from the Ag–Au-rich matrix phase but not from the Pt–Cu-rich second phase.

The purpose of this study was to systematically study the corrosion behaviour of a series of quaternary gold–silver–copper–zinc alloys using dc potentiodynamic scanning in saline (3.5 % NaCl) environment. Phase 1 of the study consisted of conducting wide range anodic and cathodic scans in order to determine the overall characteristics of the alloy. Phase 2 of the study consisted of conducting a series of selective anodic scans and terminating the scans at different anodic potentials, in order to determine any selective dissolution occurring.

## Experimental

The samples used in this study were a selection of commercial 9 carat gold quaternary alloy (Au–Ag–Cu–Zn) wires (Golden West) with a thickness of 2 mm. Alloy compositions are

shown in Table 1. Samples were annealed after drawing by heating to 350 °C, in order to remove the effects of cold working, followed by quenching in flowing cold water. Sample surfaces were abraded with 1200G SiC paper to remove any residual oxide layers on the surface and to provide a relatively uniform surface finish to the alloy surface. Optical metallography on the gold alloys was performed by cold mounting the gold wires end on, grinding to 1200G finish using SiC paper and polishing to 1  $\mu\text{m}$  surface finish using diamond paste. Samples were then chemically etched in a modified aqua regia electrolyte containing one part concentrated  $\text{HNO}_3$  plus two parts concentrated HCl for 20 s to reveal the grain structure.

All electrochemical corrosion tests were carried out using a Voltalab 21 Potentiostat. A conventional three-electrode cell set up consisting of the working electrode, a saturated calomel electrode as the reference electrode and a platinum wire counter electrode was used. All tests were carried out in (3.5 % NaCl at room temperature (20 °C)). Specimens were initially stabilised at the free corroding potential prior to conducting potentiodynamic scans. Anodic/cathodic scans in phase 1 of the study were conducted in the range  $-1,000$  to  $+1,000$  mV at a scan rate of 1 mV/s, in order to determine the overall corrosion characteristics of the alloy. The results are presented as potentiodynamic polarisation curves in the form E vs. log I plots and Tafel Extrapolation was used to determine the corrosion rates ( $E_{\text{corr}}$  and  $i_{\text{corr}}$  values) of the system.

Phase 2 of the study consisted of conducting a series of selective anodic scans and terminating the scans at different anodic potentials. The surface morphology and composition of the alloy and corroding media were analysed using scanning electron microscopy (SEM), energy dispersive X-ray spectroscopy (EDX), X-ray photoelectron spectroscopy (XPS) and atomic absorption spectroscopy (AAS) in order to determine the corrosion mechanisms and the occurrence of any selective dissolution.

## Results

### Potentiodynamic scans for phase 1 of the study

An overlay of the potentiodynamic cathodic/anodic scans for the gold alloy samples #1, #2 and #3 in 3.5 % NaCl, are

**Table 1** Composition of gold alloys

Element	Alloy 1	Alloy 2	Alloy 3
Au	37.60	37.70	37.60
Ag	10.57	5.90	6.00
Cu	42.86	46.70	51.00
Zn	9.07	9.94	5.40

shown in Fig. 1. Analysis of the potentiodynamic scans indicate similar cathodic trends being observed on the forward scan from  $-1,000$  mV to the free corroding potential. Here,  $E_{\text{corr}}$  values were typically in the region of  $-830$  to  $-860$  mV for all alloys considered in this study.  $E_{\text{corr}}$  results as shown in Table 2 indicate little variation in potential for alloys #1 and #2, giving values of  $-864.3$  and  $-860.0$  mV respectively. However, a slightly more positive value of  $-831.6$  mV was observed for alloy #3.

Analysis of the  $I_{\text{corr}}$  data from Table 2 shows that similar values, typically  $0.4$  and  $0.8$  mA/cm<sup>2</sup> were displayed by alloys #1 and #2, respectively. In contrast the  $I_{\text{corr}}$  value for alloy #3 was significantly lower by a factor between 6X and 13X lower than the other samples, yielding a value of  $0.06$  mA/cm<sup>2</sup>.

Further potentiodynamic scanning from the free corroding potential to  $+1,000$  mV for all the gold alloys revealed the presence of a discontinuous curve in the anodic region (a series of distinct transitions showing a rise in the current density, followed by a plateau/lowering of the current density), suggesting the presence of a number of competing anodic reactions, possibly associated with the selective dissolution of the alloying elements. This is looked at in more detail in phase 2 of this study.

Further detailed analysis of the anodic portions of the curves reveal the first transition showing a pronounced rise and subsequent lowering of the current density in the  $E_{\text{corr}}$  to  $-100$  mV range was observed for all the alloy samples. In contrast, while two further transitions were observed in the ranges  $-100$  to  $+200$  mV and  $+200$  to  $+400$  mV respectively for alloys #2 and #3, only one transition was observed for alloy #1 in the voltage range  $-100$  to  $+400$  mV, as shown in Fig. 1. Further, this transition was more pronounced than the two transitions observed for alloys #2 and #3 in the same regions.

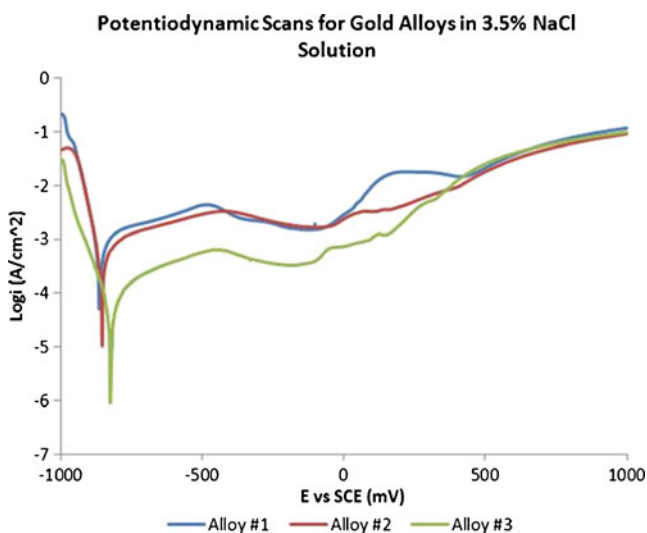


Fig. 1 Potentiodynamic scans for gold alloys in 3.5 % NaCl

**Table 2**  $E_{\text{corr}}$  and  $I_{\text{corr}}$  values for gold alloys in 3.5 % NaCl

Alloy	E <sub>corr</sub> (mV)	I <sub>corr</sub> (mA/cm <sup>2</sup> )
Alloy #1	-864.3	0.40
Alloy #2	-860.0	0.80
Alloy #3	-831.6	0.06

Structural and compositional analysis at selected anodic potentials (phase 2)

#### Scanning electron microscopy analysis of gold alloys

In this phase of the study, the gold alloy was subject to potentiodynamic scans to selected anodic potentials, corresponding to the various positions show in Fig. 2. Anodic voltages chosen for this study were selected at values (1) prior to and after the onset of the transition regions (positions A and D) and (2) at each position in the curve where a plateau/lowering in the anodic current density was observed (positions B and C). Figure 3a to d show typical SEM images of alloy #1 and alloy #3 polarised at positions A and D, respectively.

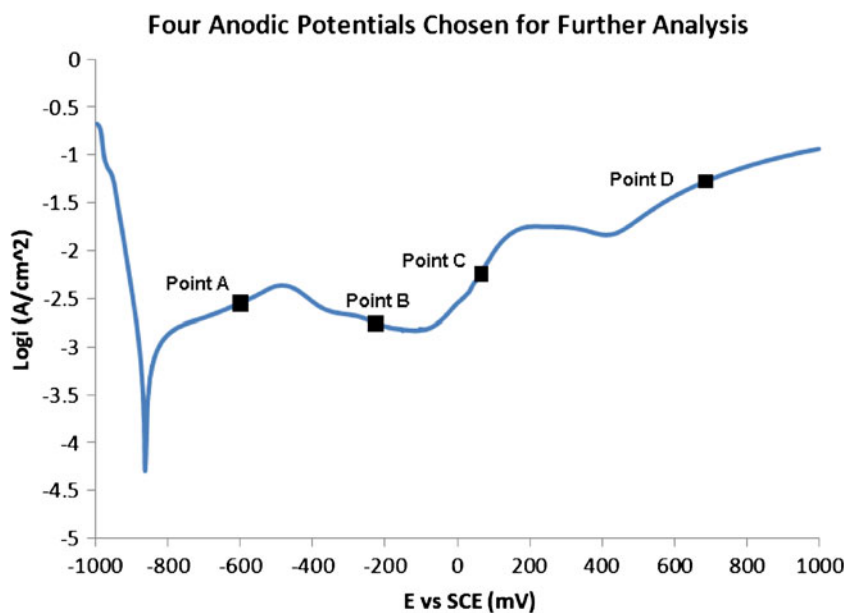
For alloy #1, the surface morphology of the micrographs indicate the presence of areas where possible dissolution of selected regions of the alloy may have occurred after polarising to position D (Fig. 3b), compared with position A (Fig. 3a). Similarly, for alloy #3, the presence of a region where corrosion, possibly associated with pitting and/or selective dissolution, resulting in the formation of porous regions is evident (Fig. 3d).

#### Energy dispersive X-ray analysis of gold alloys

Tables 3, 4 and 5 show the relative compositions of the alloys #1, #2 and #3 respectively taken at the various anodic potentials.

The results from Table 3 indicate that as the anodic potential is increased the Cu and Zn concentrations are reduced significantly, particularly after polarising to position B of the anodic curve for alloy #1 and position D for alloys #2 and #3 (Tables 4 and 5, respectively). Further, there is a significant increase in the Au and Ag content corresponding with the reduction in Cu and Zn at the various positions on the curve. The presence of oxygen was observed for all samples after polarising to all positions showing increased levels at locations corresponding with decreased Cu/Zn and increased Ag/Au concentrations. This suggests that metal oxides are formed during the polarisation process. In summary, these results would suggest that selective dissolution of the Cu and Zn has initiated at position B for alloy #1 and position D for alloys #2 and #3, evidenced by the reduced levels of Cu/Zn and increased levels of Ag/Au and oxygen.

**Fig. 2** Four anodic potentials chosen for further analysis



In addition, Table 6 shows the composition variations for alloy #2 after exposure to the environment for 20 min duration, while polarised to each of the four different anodic potentials for a constant time duration of 20 min. The results show reduced Cu and Zn levels at position D yielding compositional changes similar to those observed in Table 4.

#### *X-ray photoelectron spectroscopy analysis of gold alloys*

XPS spectra and subsequent elemental analysis from XPS of the surface of gold alloy #3 at each of the various stages of anodic polarisation are shown in Fig. 4 and Table 7, respectively. The results show that an increase in the Zn

**Fig. 3** **a** SEM image of alloy #1 polarised to position A. **b** SEM image of alloy #1 polarised to position D. **c** SEM image of alloy #3 polarised to position A. **d** SEM image of alloy #3 polarised to position D

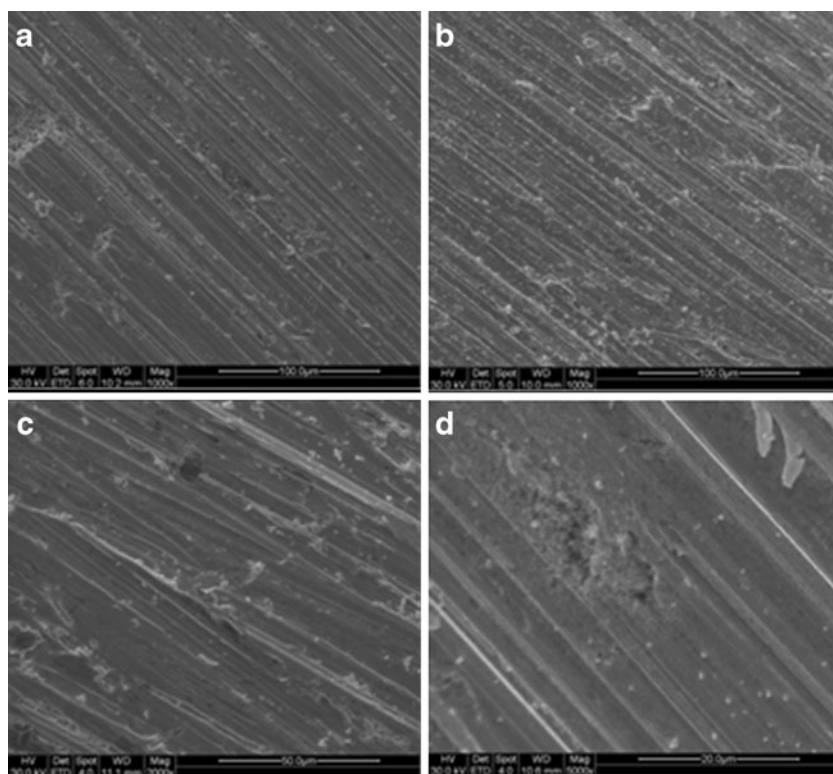


**Table 3** Elemental composition (wt.%) of alloy #1 at the four anodic potentials

	Original	Position A	Position B	Position C	Position D
O		1.71	3.46	3.79	5.58
Ag	10.57	15.03	21.4	19.43	22.14
Cu	42.86	39.02	18.67	26.39	24.52
Zn	9.07	8.08	3.44	5.29	4.69
Au	37.60	36.15	53.03	45.1	43.07

content at point C corresponding with increased O and Cl content may be attributed to localised diffusion of Zn and the formation of oxides and/or chlorides of Zn at the surface. Further, at point D, the increase in Cu concentration accompanied by further increase in Cl and O content may be associated with (1) localised Cu diffusion and the formation of oxides and/or chlorides of Cu or (2) the dissolution and subsequent re-formation of Cu or Cu chlorides/oxides due to reduction of Cu ions. The reduction of copper ions to metallic copper will be facilitated by the presence of Zn at the surface through a galvanic replacement process. In addition, the Zn concentration decreased at position D, supporting the dissolution of Zn from the alloy at this point.

The Cu spectra of gold alloy #3 at positions A and D of the cyclic polarization curve, as shown in Fig. 5, reveal that the peak binding energy (BE) of Cu2p increases from 932.72 at position A (scan A) to 935.39 at position D (Scan B), which correspond to Cu and Cu(OH)<sub>2</sub>, respectively. These results support the theory that oxidised copper species are formed as part of the corrosion/dissolution process. The presence of shake up satellite peaks also support that the formation of Cu(OH)<sub>2</sub> occurs.

#### Atomic absorption spectroscopy analysis of gold alloys

The results of the atomic absorption spectroscopy analysis for Cu and Zn ions from all three gold alloys after being anodically polarised to position D are shown in Table 8. These results further confirm the dissolution of Cu and Zn into the solution. Further, the highest concentration of Cu

**Table 4** Elemental composition (wt.%) of alloy #2 at the four anodic potentials

	Original	Position A	Position B	Position C	Position D
O		1.19	2.36	1.47	2.87
Ag	5.90	12.93	8.76	6.66	8.08
Cu	46.70	14.02	41.55	42.42	16.23
Zn	9.94	2.49	7.96	8.41	3.13
Au	37.70	68.47	39.01	40.76	69.69

**Table 5** Elemental composition (wt.%) of alloy #31 at the four anodic potentials

	Original	Position A	Position B	Position C	Position D
O		1.82	3.07	2.88	2.99
Ag	6.00	7.81	7.18	8.75	12.82
Cu	51.00	44.25	33.86	42.7	16.42
Zn	5.40	8.43	7.44	7.83	2.57
Au	37.60	37.69	48.45	37.08	65.21

and Zn cations (78.8 mg/L of Cu<sup>2+</sup> and 15.6 mg/L of Zn<sup>2+</sup> present in the final solution after completion of testing) was observed in the gold alloy #1 solution and the least in gold alloy #3, suggesting that increased selective dissolution was observed for alloy #1 compared with alloys #2 and #3

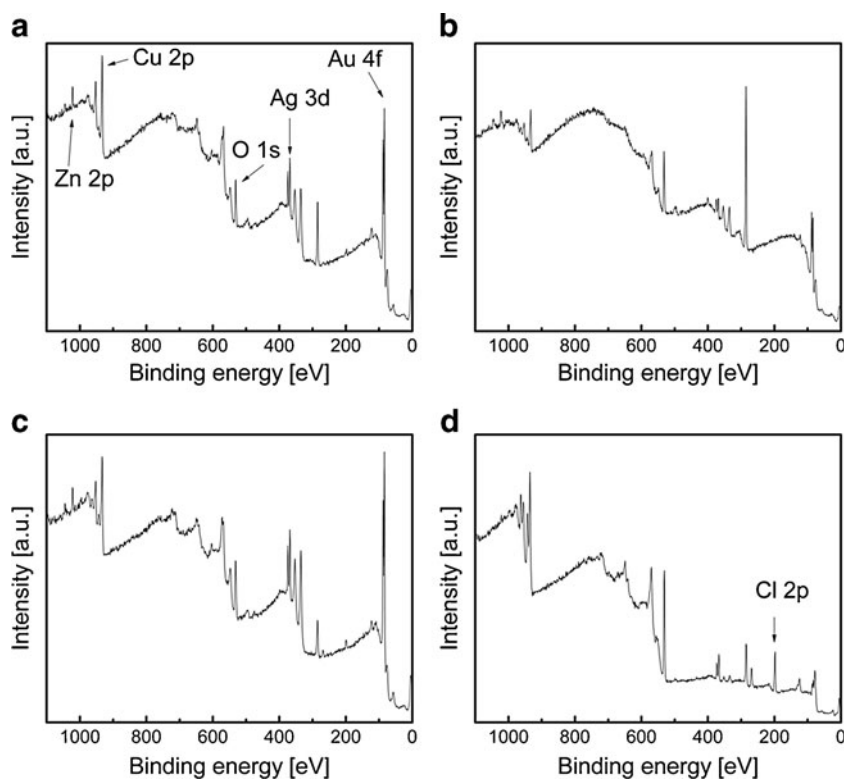
#### Corrosion behaviour of gold alloys under non-accelerated (free corroding) conditions

Corrosion studies under non-accelerated conditions were also carried out, whereby all three alloys were immersed for 240 h in the environment under free corroding conditions. Analysis of the samples using SEM imaging and EDX analysis revealed dense corrosive products were formed on the surface of alloys #1 and #3 (Fig. 6) in contrast to more severe corrosion/selective dissolution being observed on sample #2 (Fig. 7). Table 9 is a summary of the surface EDX analysis of all three alloys after 240 h immersion confirming some of the results and observations from the accelerated tests as indicated in section “**Structural and compositional analysis at selected anodic potentials (phase 2)**”. The higher levels of oxygen and chloride associated with alloys #1 and #3 compared with alloy #2 would indicate the dense corrosion products on the surface are oxides/chlorides of Zn and Cu, possibly in the form of ZnO, CuCl<sub>2</sub> and CuCl. In contrast, dissolution of gold alloy #2 may be responsible for the lower amounts of O and Cl being detected (Fig. 8).

**Table 6** Elemental composition (wt.%) of alloy #2 after 20 min exposure to the environment at the four anodic potentials

	Original	Position A	Position B	Position C	Position D
O		1.99	3.14	2.78	9.1
Ag	5.90	6.26	8.49	7.88	9.56
Cu	46.70	45.02	43.69	42.19	23.37
Zn	9.94	8.97	7.65	8.35	3.47
Au	37.70	37.75	37.03	38.8	54.5

**Fig. 4** XPS spectra for gold alloy #3 at the various anodic polarisation potentials



### General Discussion on the Selective Dissolution of the Gold Alloys

Influence of gold chemistry and metallurgy on selective dissolution

Another important factor in the dissolution mechanism of gold alloys is the metallurgy of the alloy, specifically if the alloy contains a homogeneous or heterogeneous structure. Selective dissolution of homogeneous binary Au–Ag and Au–Cu alloys has been studied in detail [3]. Mechanisms for attack of the selective dissolution of the more active atoms (alloying species) is influenced by a number of factors to include (1) the activation energy or overpotential to remove these species; (2) presence of these atoms within the lattice,

for example at kink sites where removal of atoms is easier and (3) migration of lattice vacancies and diffusion of the more noble species (gold) to form clusters/islands. For high gold alloys, passivation is ultimately achieved, however for low gold alloys, micromorphological studies have shown ultimate disintegration of the alloy may occur through the development of tunnels or pits [14].

For heterogeneous alloys, the mechanism of dissolution becomes more complex as the tendency for corrosion for the different phases present may differ depending on the chemistry of the phases. For example the preferential corrosion of Ni-rich phases containing less gold in Ni-based white gold alloys, may occur when exposed to acid. It was further stated [3] that while this form of corrosion may occur due to the presence of heterogeneous phases in ternary, low caratage Au–Ag–Cu alloys, no studies have been reported of this effect in quaternary Au–Ag–Cu–Zn alloys (Fig. 9).

A review of the metallurgy of ternary Au–Ag–Cu alloys has shown that the phases formed can be quite complex [17–19]. For simple Au–Cu alloys, the existence of four phases are possible, namely  $\alpha$  (Au, Cu) solid solution,  $\text{Au}_3\text{Cu}$ ,  $\text{AuCu}$  and  $\text{AuCu}_3$  intermetallics [17]. Given that the percentage of Cu in the alloys in this study lies between 42 and 51 %,  $\alpha$  (Au, Cu) and  $\text{AuCu}$  are the most likely phases to be present and possibly  $\text{Au}_3\text{Cu}$ . For simple Au–Ag alloys, a solid solution  $\alpha$  (Au, Ag) is expected [18, 19] and for simple Cu–Ag alloys, a two-phase alloy is expected containing immiscible Cu-rich and Ag-rich ( $\alpha(\text{Au–Cu})$  and  $\alpha(\text{Ag–Ag})$ ) solutions, respectively [18, 19]. For the Au–

**Table 7** Elemental composition (at%) from XPS of gold alloy #3 at the four anodic polarisation potentials

Element	Position A (at%)	Position B (at%)	Position C (at%)	Position D (at%)
Au	6.5	1.5	7.8	0.3
C	63.4	81.1	47.4	36.4
Cl	0	0	5.6	16.2
Ag	2.6	0.5	2.9	0.9
O	19.3	13.2	27.6	33.8
Cu	6.6	2.2	6.6	11
Zn	1.7	1.4	2.3	0.3

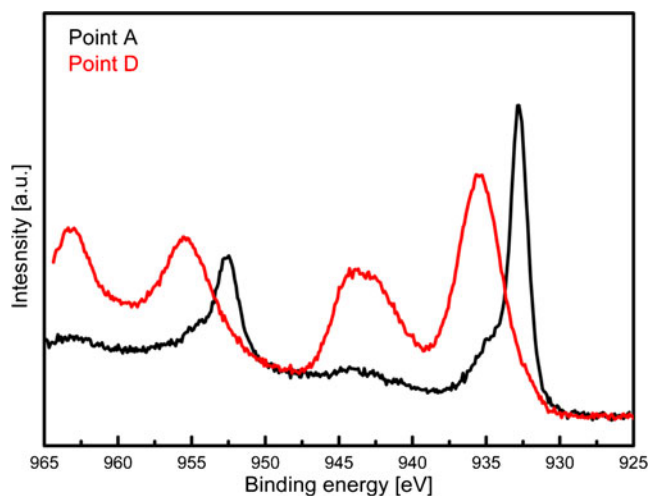


**Fig. 5** Cu2p binding energy spectra of Cu on the surface of alloy #2 at position A and D of the polarisation curve

Ag–Cu ternary alloy, according to McDonald and Sistare [13], the parameter  $Ag'$ , defined as the ratio of Ag to Ag + Cu content, is one factor, in addition to carat value, which is important in determining the stable phases in this alloy.

In the current study, the  $Ag'$  values were calculated as 0.20 for alloy #1 and 0.11 for alloys #2 and #3. This suggests that while alloys #2 and #3 may be homogeneous consisting of a solid solution alloy,  $\alpha$ , of Cu, Ag and Au, alloy #1 may be heterogeneous, containing an immiscible silver-rich (Au–Ag) phase (and possibly the presence of a Cu-rich  $\alpha$  (Cu–Au) phase cannot be neglected, although this is more prominent for alloy systems with  $Ag'$  value 0.25–0.75) [18]. However, the presence of Zn can tend to reduce the volume of solid state immiscibility in the ternary phase diagram, driving the microstructure towards that of a homogeneous solid solution [18, 19]. This has been systematically studied and predicted by Klotz [20] who has used computer modelling techniques, particularly thermodynamic simulation to allow for calculation of phase diagrams for alloy design, heat treatment processes and understanding of segregation particularly the effects of two-phase field contraction.

Optical and scanning electron micrographs of the metallographically prepared (polished and etched) surface of alloy #1 as shown in Figs. 11 and 12 respectively, reveal the presence of a microstructure consisting of grains varying in size ranging from 25 to 100  $\mu\text{m}$  diameter. EDX analysis of the light and dark regions, as shown in Fig. 12, shows no

**Table 8** AAS results for Cu and Zn cation concentrations

Ion	Alloy #1	Alloy #2	Alloy #3
Cu <sup>2+</sup> (mg/L)	78.8	18.6	12.2
Zn <sup>2+</sup> (mg/L)	15.6	4.4	2.8

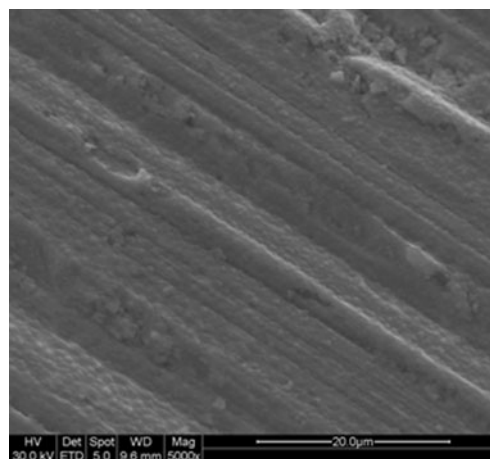


**Fig. 6** SEM image of alloy #3 after 240 h in 3.5 NaCl

variation in the concentration of the major alloying elements (Ag, Au, Cu and Zn). This suggests the presence of a homogeneous solid solution, the light and dark regions attributed to etch induced contrast rather than variations in elemental composition. In addition to the major alloying elements, peaks from the EDX analysis, were identified and associated with the presence of Si and ruthenium (Ru) and/or iridium (Ir), confirming the presence and use of these minor alloying additions as grain refining agents, a practice common to commercial production of gold alloys. The findings from the metallographic studies compliment the prediction of phases present from calculations of  $Ag'$  values, in so far as a homogeneous phase structure was expected from all alloys, even from alloy #1 with an  $Ag'$  value approaching that for alloys where binary phase structures may exist.

Identifying the possible distribution of phases and the formation of homogeneous/heterogeneous structures is of importance in determining the corrosion mechanism of these

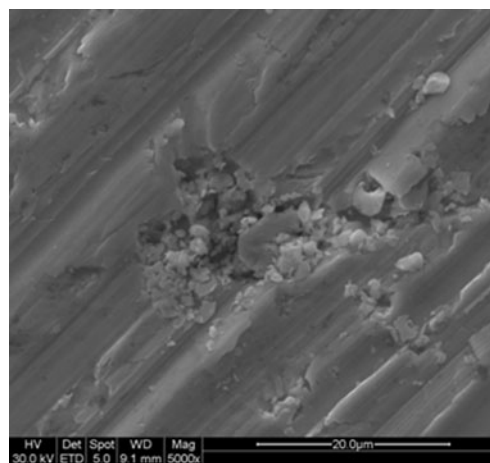


**Fig. 7** SEM image of alloy #2 after 240 h in 3.5 NaCl

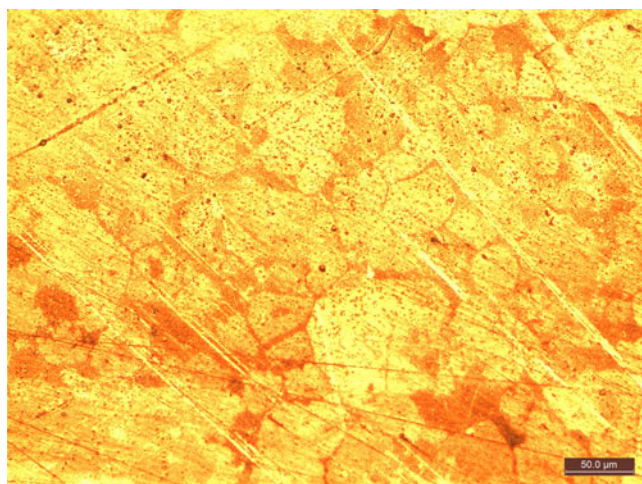
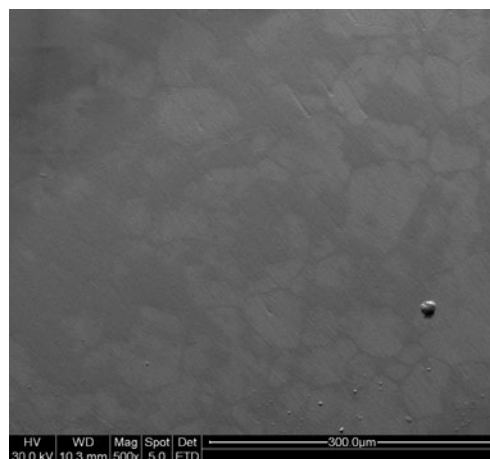
**Table 9** EDX analysis of gold alloys after 240 h immersion in 3.5 % NaCl solution

Element	Alloy #1	Alloy #3	Alloy #4
O	10.72	1.66	12.22
Cl	4.83	1.39	5.04
Ag	7.91	6.32	9.34
Cu	23.32	26.47	21.04
Zn	3.47	5.36	3.69
Au	49.75	58.8	48.66

alloys. While this may not influence the overall corrosion behaviour of the alloys it will certainly have an influence on the mechanism by which these alloys corrode, whether through the removal of active species and diffusion/clustering of more noble species, as for alloys with a homogeneous structure, or if preferential corrosion occurs of entire phases enriched in active constituents.

#### Effect of composition on the corrosion behaviour of gold alloys

Corrosion of gold jewellery normally involves selective attack of the less noble alloy constituents and it is well established [3] that while the addition of silver and other base metals reduces the corrosion resistance of gold, this is not significant as long as the gold content of the alloy remains greater than 50 at% (corresponding to 15.6 carat Au–Ag alloys and 18 carat for Au–Cu alloys). However, it should be noted that this “50 at% rule of thumb” is very general and simplistic as Corti [21] reported that tarnishing of 22 carat gold can occur under relatively severe corrosion conditions in general service, as evidenced by the presence of a blackened surface on the alloy.

**Fig. 8** Optical micrograph of alloy #1 etched in aqua regia (X340 mag)**Fig. 9** SEM image of alloy #1 etched in aqua regia

The reported composition of Au in all three low carat alloys in the current study is around the 37 at%, thus making them susceptible to corrosion, particularly selective dissolution. It would appear that variations in alloying additions into the alloys not only affect the overall anodic region of the curve but also the resultant  $E_{\text{corr}}$  and  $I_{\text{corr}}$  values, as shown in Fig. 1 and Table 2.

Firstly reduced Cu (and increased Ag) content may be responsible for (1) increasing the intensity of the second transition with respect to a pronounced increase in the current density range at the commencement of this transition at  $-100$  mV for alloy #1 compared with alloys #2 and #3 and (2) suppressing the third transition in the anodic region between  $+200$  to  $+400$  mV observed in alloys #2 and #3 but not alloy #1. This would suggest that reduced Cu content is responsible for intensifying the dissolution of the alloying species occurring at around  $-100$  mV (alloy #1) and further, increased Cu content promotes the dissolution of species occurring at  $+200$  mV.

Secondly, a reduction in the Zn content from approximately 9–10 % to 5.4 % may have been responsible for the observed more positive  $E_{\text{corr}}$  value and lower  $I_{\text{corr}}$  value observed for alloy #3 compared with the other alloys. This would suggest that the Zn content in the alloy is an important factor regarding influencing the overall corrosion properties of the alloy. Further, correlations exist between the observed  $I_{\text{corr}}$  values and results from the free corroding tests conducted. Here, the lower  $I_{\text{corr}}$  values observed for alloys #1 and #3 can be attributed to the presence of dense corrosion products on the surface as evidenced in Fig. 6 and the higher levels of O and Cl from EDX analysis compared with alloy #2 showing lower levels of O and Cl and evidence of selective dissolution (Fig. 7). This may be associated with the higher Zn content as compared with alloy #3, combined with higher Cu content as compared with alloy #1, making this alloy the most susceptible to attack and subsequent dissolution.



## Dissolution mechanisms for gold alloys

The electrochemical potentials of Au, Ag, Cu and Zn are reported with values of +1,498, +799, +337 and -763 mV vs normal hydrogen electrode [22]. While these values represent ideal conditions for metals under reversible conditions in a solution of its own ions at unit activity, combined with the galvanic series for metals and alloys in salt water, they give an indication of the relative differences in the degree of activeness/inertness of each of the alloying elements [22]. In summary, it is anticipated that dissolution of Zn species would occur first, followed by Cu, then Ag and finally Au.

For sample #1, at position A (-600 mV vs SCE), approximately 250 mV more positive than the  $E_{\text{corr}}$  value, the Cu and Zn levels from EDX analysis suggest no leaching out of these species, although the formation of some oxides is evidenced. At position B (-200 mV vs SCE), the selective dissolution of both Cu and Zn, resulting in regions depleted of these species and enriched in Au and Ag, suggests that both these corrosion reactions have occurred within the 400 mV band between test positions A and B. While Zn is expected to leach out initially, the results cannot confirm this theory. While the EDX results suggest no further dissolution of species is observed upon further testing at positions C and D, the anodic potentiodynamic scans suggest further dissolution of species at point C and D. This may indicate either (1) stabilisation of the alloy with respect to alloy composition or (2) leaching out/oxidation of all species (Au and Ag in addition to Cu and Zn) thus maintaining constant alloy composition. Increase in oxide composition may suggest further oxides are formed indicating activity at these potentials.

In contrast, for alloys #2 and #3, the EDX results indicate suppression of the dissolution of Zn and Cu until more anodic potentials are achieved (between +100 mV vs SCE at point C and +600 mV vs SCE at point D). However, the anodic polarisation scans suggest that activity, possibly associated with dissolution and/or oxide formation is taking place though not to the extent as for alloy #1.

It appears that the overall corrosion characteristics of the alloys are determined by the extent of anodic reactions which induce (1) formation of oxides on the alloy surface; (2) dissolution of Zn and Cu species and (3) relative combinations of the first two. Dissolution of Zn and Cu ions appears to dominate in alloy #1, initiating in the early phase of the anodic region, as evidenced by increased concentrations of Zn and Cu from the AAS analysis of the corrosion solutions and low O and Cl concentrations from EDX analysis under free corroding conditions. This may be attributed to the possible formation of heterogeneous phases, with dissolution of Cu-rich phases and Zn regions in alloy #1. However, increased Zn levels for this alloy may also be a

contributing factor. In contrast, the formation of a homogeneous phase, likely to be evident in alloys #2 and #3, may delay dissolution of Zn and Cu species until higher anodic potentials are achieved.

The high corrosion rates observed for alloy #2 can be attributed to the lack of protective scales forming, as evidenced by the low O and Cl concentrations from the free corrosion studies. In contrast the formation of protective oxide scales (higher O and Cl levels) may account for the lower corrosion rates observed for alloy #3, which may also be attributed to higher Cu concentrations in the alloy. Further analysis from XPS suggests that at point C (approximately -200 to +100 mV vs SCE.), chlorides start to form and oxide concentrations increase suggesting the formation of stable copper oxides/chlorides and or zinc oxides/chlorides. At higher anodic potentials (+100 mV to +600 mV vs SCE) reduced Zn content could be attributed to further dissolution of Zn and/or breakdown of any stable Zn oxide layers formed. Likewise the increased Cu content could be attributed to dissolution/replating back of copper and subsequently forming copper oxides. A uniform distribution of copper and zinc oxide on the surface may be responsible for masking the Au and Ag present and thus explaining the low levels of Ag and Au detected at point D.

Correlation of the corrosion results with previous corrosion, SCC and tarnish resistance studies

The general findings from this study are that alloying additions influence the corrosion behaviour of the alloy by inducing selective dissolution of the active species, reduced corrosion resistance being observed with increased Zn levels. Laub and Stanford [15] observed a correlation between the composition of five low-carat gold dental alloys and the resultant corrosion and tarnishing results. As the gold content increased from 40 to 59.5 %, a reduction in the electrochemical corrosion rates was observed, in addition to no tarnishing or corrosion from clinical trials being observed for higher gold content alloys. While, the increased levels of gold are primarily responsible for improved corrosion and tarnish resistance, corrosion was attributed to the presence of the more active alloying additions of Cu and Ag, producing Ag-rich and Cu-rich regions which are more susceptible to corrosion. Rapson [3] reported desirable microstructural features for improved resistance to tarnish and corrosion in low-carat gold alloys are due to the presence of large grains, a minimum of phase separation and absence of precipitated and ordered phases, although it was uncertain if these conditions can apply to low-carat gold alloys containing significant percentages of Zn.

Merriman and co-workers [23] reported the time to fracture during SCC tests was much higher for the 18 carat gold alloys (several hundred hours) compared with those for

lower-carat gold alloys (several minutes). In addition, the corrosion rates of the low-carat gold alloys were attributed to selective dissolution of the alloying additions, whereby dissolution of Zn occurred initially, followed by dissolution of Cu, Ni and Pd, leaving a gold-enriched layer. Hence alloys containing Zn experienced the highest corrosion rates, due to the lower oxidation potential of Zn compared with other alloying additions. Rapson [3] stated that the susceptibility of 14 carat quaternary Au–Ag–Cu–Zn alloys to SCC was influenced considerably by both the Zn content and heat treatment. Neumeier and co-workers [10] compared the SCC behaviour of a series of 9 carat gold alloys with varying compositions of Ag, Cu and Zn. Their studies revealed that SCC behaviour appeared to be related to differences in Zn content rather than Cu content, for alloys containing the same Au and Ag content. Increased resistance to SCC was observed for gold alloys with lower Zn content. They attributed this to the low Zn content alloy promoting the formation of a heterogeneous, dual-phase structure, being more resistant to SCC, whereas at higher Zn content, the formation of a homogeneous, single-phase was promoted, thus rendering the alloy more susceptible to SCC.

In the current study the Au content was kept constant while Ag, Cu and Zn contents varied. Hence, any changes to the corrosion behaviour are predominantly dependent on the alloying additions themselves. It is clear that previous work has shown Zn content in the gold alloys to be detrimental to the corrosion rates and SCC resistance. The findings from this study correlate well with previous work, the worst corrosion resistance being observed for alloy #2 with higher Zn/lower Cu content, compared with alloy #3. It is possible that the best corrosion behaviour observed from alloy #3, being attributed to favourable Zn/Cu ratio (low Zn content and increased Cu content), may also result in these alloys showing improved SCC resistance and possibly improved tarnish resistance compared with the other alloys, although further studies would be required to confirm this theory.

## Conclusions

1. Potentiodynamic scans conducted on all gold alloys in 3.5 % NaCl solution indicate the presence of similar discontinuous curves in the anodic region (a series of distinct transitions showing a rise in the current density, followed by a plateau), most likely due to selective dissolution of the alloying elements.
2. Phase 1 of the study revealed alloy #3 showed slightly more positive corrosion voltage ( $E_{\text{corr}}$ ) value and lower corrosion current ( $I_{\text{corr}}$ ) value (between 6X to 13X lower) than alloys #1 and #2. This may be associated with reduced Zn and increased Cu levels within the alloy

promoting the formation of dense, protective coating products on the surface.

3. Higher corrosion rates as observed for alloy #2 and to a lesser extent, alloy #1, may be associated with increased Zn and reduced Cu levels in the alloy promoting susceptibility to attack and subsequent selective dissolution.
4. Phase 2 studies revealed selective dissolution of Cu and Zn species from alloy #1 occurred early on in the anodic region of the polarisation curve. This was supported by the increased Zn and Cu levels found in solution and reduced O and Cl levels observed on the alloy surface. This may be attributed to the possible formation of a heterogeneous phase structure.
5. Dissolution of Zn and Cu species is suppressed, leaching at more positive anodic potentials, for alloys #2 and #3 compared with alloy #1. This may be attributed to the possible existence of a homogeneous phase structure that delays dissolution.
6. The corrosion behaviour of the alloys is determined by the extent of anodic reactions which induce (1) formation of oxide scales on the alloy surface and or (2) dissolution of Zn and Cu species. In general, the improved corrosion characteristics of alloy #3 can be attributed to the favourable composition of Zn/Cu in the alloy and thus favourable microstructure promoting the formation of protective oxide/chloride scales and reducing the extent of Cu and Zn dissolution.

**Acknowledgement** The authors would like to acknowledge Prof. Suresh Bhargava for provision of gold alloy samples. The authors further acknowledge the facilities and technical assistance of the Australian Microscopy and Microanalysis Research Facility at the RMIT Microscopy and Microanalysis Facility

**Open Access** This article is distributed under the terms of the Creative Commons Attribution License which permits any use, distribution, and reproduction in any medium, provided the original author(s) and the source are credited.

## References

1. Ott D (2002) Optimising gold alloys for the manufacturing process—advantages and disadvantages of small alloying additions. *Gold Technol* 34:37–44
2. Randin J-P (1988) Electrochemical assessment of the tarnish resistance of decorative gold alloys. *Surf Coat Technol* 34:253–275
3. Rapson WS (1996) Tarnish resistance, corrosion and stress corrosion cracking of gold alloys. *Gold Bull* 29:61–69
4. Alvarez MG, Fernández SA, Galvele JR (2000) Stress corrosion cracking in single crystals of Ag–Au alloy. *Corros Sci* 42:739–752
5. Chen JS, Salmeron M, Devine TM (1993) Intergranular and transgranular stress corrosion cracking of Cu–30Au. *Corros Sci* 34:2071–2097

6. Farina SB, Duffo GS, Galvele JR (2007) Effect of cations on stress corrosion cracking: Ag-40Cd alloy in silver ion aqueous solutions containing a variety of foreign cations. *Corros Sci* 49:1687–1695
7. Alvarez MG, Fernandez SA, Galvele JR (2002) Effect of temperature on transgranular and intergranular stress corrosion crack velocity of Ag–Au alloys. *Corros Sci* 44:2831–2840
8. Duffo GS, Farina SB, Galvele JR (2004) Stress corrosion cracking of 18 carat gold. *Corros Sci* 46:1–4
9. Dugmore JMM, DesForges CD (1979) Stress corrosion in gold alloys. *Gold Bull* 4:140–144
10. Neumayer B, Hensler J, O'Mullane AP, Bhargava SK (2009) A facile chemical screening method for the detection of stress corrosion cracking in 9 carat gold alloys. *Gold Bull* 42:209–214
11. Bray W (1978) Gold working in ancient America. *Gold Bull* 4:136–143
12. Forty AJ (1979) Corrosion micromorphology of noble metal alloys and depletion gilding. *Nature* 282:597–598
13. Nakagawa M, Matsuya S, Ohta M (1992) Effect of microstructure on the corrosion behaviour of dental gold alloys. *J Mater Sci Mater Med* 3:114–118
14. Forty AJ (1981) Micromorphological studies of the corrosion of gold alloys. *Gold Bull* 14:25–35
15. Laub LW, Stanford JW (1981) Tarnish and corrosion behaviour of dental gold alloys. *Gold Bull* 14:13–18
16. Fujita T, Shiraishi T, Takuma Y, Hisatsune K (2011) Corrosion resistance evaluation of Pd-free Ag–Au–Pt–Cu dental alloys. *Dent Mater J* 30:136–142
17. Okamoto H, Chakrabarti DJ, Laughlin DE, Massalski TB (1987) The Au–Cu (gold–copper) system. *Bull Alloy Phase Diagr* 8:454–473
18. McDonald AS, Sistare GH (1978) The metallurgy of some carat gold jewellery alloys part I—coloured gold alloys. *Gold Bull* 11:66–73
19. Rapson WS (1990) The metallurgy of the coloured carat gold alloys. *Gold Bull* 23:125–133
20. Klotz UE (2012) Computer simulation in jewellery technology—meaningful use and limitations. *Proc Santa Fe Symp* 2012:297–319
21. Corti CW (2000) High carat golds do not tarnish? *Proc Santa Fe Symp* 2000:29–55
22. Fontana MG (1986) *Corrosion engineering*, 3rd edn. McGraw-Hill pp 42–43
23. Merriman CC, Bahr DF, Grant Norton M (2005) Environmentally induced failure of gold jewellery alloys. *Gold Bull* 38:113–119